Coherence Length of Cold Exciton Gases in Coupled Quantum Wells

Sen Yang, A. T. Hammack, M. M. Fogler, and L. V. Butov
Department of Physics, University of California at San Diego, La Jolla, California 92093-0319, USA

A. C. Gossard
Materials Department, University of California at Santa Barbara, Santa Barbara, California 93106-5050, USA

(Received 27 June 2006; published 31 October 2006)

A Mach-Zehnder interferometer with spatial and spectral resolution was used to probe spontaneous coherence in cold exciton gases, which are implemented experimentally in the ring of indirect excitons in coupled quantum wells. A strong enhancement of the exciton coherence length is observed at temperatures below a few Kelvin. The increase of the coherence length is correlated with the macroscopic spatial ordering of excitons. The coherence length at the lowest temperature corresponds to a very narrow spread of the exciton momentum distribution, much smaller than that for a classical exciton gas.

DOI: 10.1103/PhysRevLett.97.187402 PACS numbers: 78.67.De, 71.35.−y, 73.21.Fg

Coherence of excitons in quantum wells attracts considerable interest. It has been intensively studied by four-wave-mixing [1], coherent control [2], and interferometric and speckle analysis of resonant Rayleigh scattering [3–5]. In all these experiments, exciton coherence was induced by a resonant laser excitation and was lost within a few pico seconds (ps) after the excitation pulse due to exciton-exciton and exciton-phonon collisions and due to inhomogeneous broadening by disorder.

Another fundamentally interesting type of coherence is spontaneous coherence (not driven by the laser excitation). Studies of spontaneous coherence of excitons require implementation of cold exciton gases, see below. This can be achieved with indirect excitons in coupled quantum wells (CQW) [6]. Taking advantage of their long lifetime and high cooling rate, one can realize a gas of indirect excitons with temperature well below 1 K and density in excess of 10^{10} cm^{-2} [6]. For comparison, the crossover from classical to quantum gas occurs at $T_{\mathrm{dB}} = 2\pi\hbar^2 n/(mgk_B)$ and $T_{\mathrm{dB}} \approx 3$ K for the exciton density per spin state $n/g = 10^{10}$ cm^{-2} (exciton mass $m = 0.22m_0$, and spin degeneracy $g = 4$ for the GaAs/AlGaAs QWs [6]). Note that at this density, $na_B^2 \sim 0.1$ and, therefore, excitons are interacting hydrogenlike Bose particles [7] ($a_B \approx 20$ nm is the exciton Bohr radius [8]).

Spontaneous coherence can be experimentally studied using nonresonant laser excitation so that coherence is not driven by the laser. However, nonresonant excitation may lead to strong heating of the excitons in the excitation spot [9]. Therefore, in this Letter, we study coherence in the external exciton rings [10], which form far away from the excitation spot [Fig. 1(c)], at the border between the electron- and hole-rich regions [11,12]. The external ring of indirect excitons in CQW is the region where the exciton gas is cold: The excitons in the ring are formed from well-thermalized carriers, and their temperature essentially reaches that of the lattice. The cold exciton gas in the external ring can form a macroscopically ordered exciton state (MOES)—an array of beads with spatial order on a macroscopic length [10]. The MOES appears abruptly along the ring at T below a few Kelvin.

In this Letter, we report on emergence of spontaneous coherence of excitons at low temperatures. The exciton coherence length increases strongly below a few Kelvin, in concert with the macroscopic spatial ordering of excitons. At the lowest T, the measured coherence length corresponds to a very narrow spread of exciton momentum distribution, much smaller than that for a classical exciton gas.

Spontaneous coherence of excitons translates into coherence of the emitted light [13–16]. To probe it, several optical experimental techniques have been proposed: a second-order optical response [13], a Hanbury Brown–Twiss interferometry [14,15], and a speckle analysis at off-resonant excitation [16]. Our technique is based on

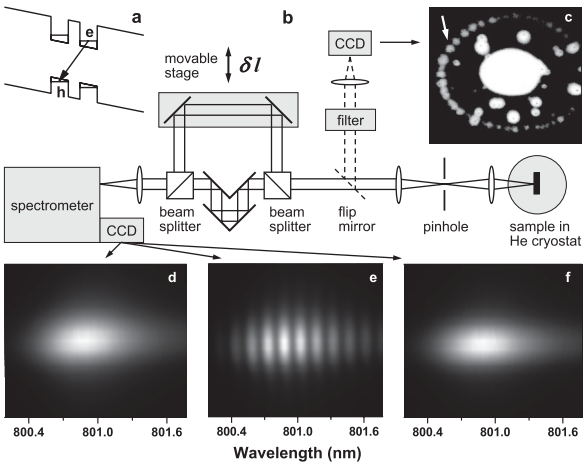

FIG. 1. (a) The CQW band diagram. (b) Scheme of MZ interferometer with spatial and spectral resolution. (c) The pattern of indirect exciton PL. The area of view is 280 × 250 μm. Spectra for the left (d), right (f), and both (e) arms of the MZ interferometer. The light was selected from the center of the arrow-marked MOES bead. The length of view (vertical axis) is 25 μm. $T = 1.6$ K, $V_g = 1.24$ V, $D = 25$ μm, $\delta l = 4.2$ mm, and $P_{\mathrm{ex}} = 0.7$ mW for all the data.

measuring the first-order coherence function of the electric field $E(t, \mathbf{r})$ of the light emitted by excitons. This quantity is defined by [17,18]

$$g(t, \mathbf{r}) = \langle E(t' + t, \mathbf{r}' + \mathbf{r}) E(t', \mathbf{r}') \rangle / \langle E^2(t', \mathbf{r}') \rangle. \quad (1)$$

(local ergodicity in space and time is assumed). The linear technique allows us to work with the low level optical signals of the spatially resolved photoluminescence (PL).

Our experimental setup [Fig. 1(b)] is a variant of Mach-Zehnder (MZ) interferometry with new ingredients. First, we added spatial resolution by collecting the light only from a selected area of size $D/M_1 = 2$–10 μm in the middle of a MOES bead. This was done by placing a pinhole of diameter $D = 10$–50 μm at the intermediate image plane of magnification $M_1 = 5$. Second, we added the frequency resolution by dispersing the output of the MZ interferometer with a grating spectrometer. (The image was further magnified by the factor $M_2 \approx 2$ after the pinhole.) The output of the spectrometer was imaged by a nitrogen cooled CCD. The MZ delay length δl was controlled by a piezo-mechanical translation stage. The PL pattern of the indirect excitons [Fig. 1(c)] was also imaged with the pinhole removed and the image filtered at the indirect exciton energy (dashed path in Fig. 1(b)]. The excitation was supplied by HeNe laser at 633 nm (the laser excitation spot with FWHM 7 μm is in the center of the exciton ring. The excitation was 400 meV above the indirect exciton energy and well separated in space; therefore, no laser-driven coherence was possible in the experiment. The CQW structure with two 8 nm GaAs QWs separated by a 4 nm $Al_{0.33}Ga_{0.67}As$ barrier was grown by MBE. For the applied external gate voltage $V_g \approx 1.2$ V, the ground state is an indirect exciton with a lifetime $\tau_{rec} \sim 40$ ns (details on the CQW structures can be found in [6]).

An example of the measured interference pattern is shown in Fig. 1(e). The light was collected from the center of a bead shown in Fig. 1(c) by the arrow. (While all interference profiles in the Letter refer to this spot, similar profiles were measured from other spots on the ring.) The modulation period $\delta\lambda$ of the CCD signal I was deduced from the locations of the satellite peaks of Fourier transform of I, Fig. 2(a). It was found to obey the expected dependence $\delta\lambda = \lambda^2/\delta l$ (see Fig. 2(b) and below). To quantify the amplitude of the modulations, we computed their visibility factor $V = (I_{max} - I_{min})/(I_{max} + I_{min})$ using a method based on the Fourier analysis [Eq. (3)]. The visibility factor was examined for a set of δl and T.

The main experimental result is presented in Fig. 3(c): Visibility of the interference fringes sharply increases at temperatures below a few Kelvin. This contrasts with the T-independent V of the direct exciton emission measured at the excitation spot center at $T = 2$–10 K.

Let us proceed to the data analysis. Recall that for a classical source with a Lorentzian emission lineshape, the first-order coherence function [Eq. (1)] at the coincident points is given by $g(t, \mathbf{r} = 0) = \exp(-t/\tau_c)$, where τ_c is the inverse linewidth. By analogy, we assume the

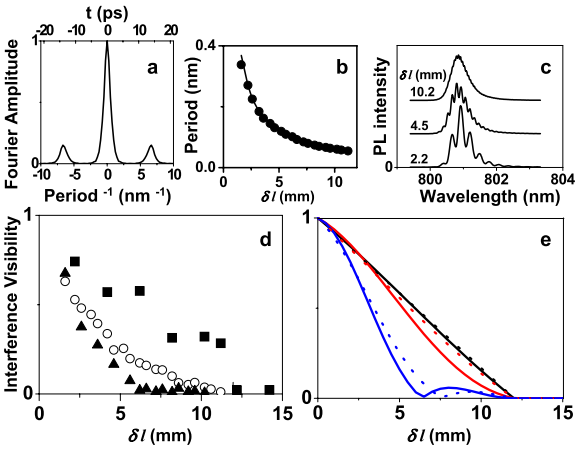

FIG. 2 (color online). (a) The Fourier transforms of the CCD signal for $D = 50$ μm and $\delta l = 4.2$ mm. (b) Period of the interference fringes vs δl. Solid line: fit to $\delta\lambda = \lambda^2/\delta l$. (c) Interference profiles for $D = 50$ μm and $\delta l = 2.2$, 4.5, and 10.2 mm. (d) Measured and (e) calculated visibility of the interference fringes vs δl for $D = 50$ (triangles), 25 (circles), 10 μm (squares), and $M_2 = 1.7$. Solid and dotted lines in (e) correspond to the Eqs. (7) and (9), respectively. $T = 1.6$ K, $V_g = 1.24$ V, $P_{ex} = 0.7$ mW for all the data.

r-dependence in the form $g(t, \mathbf{r}) = g(t, 0)\exp(-r/\xi)$, where ξ is the coherence length. Our goal is to deduce ξ from the contrast of the periodic modulations in the CCD image, Fig. 1(e). Consider the central row of that image. Let x be a coordinate along this row and let x_0 be the position of the diffraction maximum for the central frequency of the emission line $\omega_0 = 2\pi c/\lambda_0$. Because of small width of this line, it is permissible to work with small deviations $\delta x = x - x_0$, $\delta\omega = \omega - \omega_0$, and $\delta\lambda = \lambda - \lambda_0$. (Thus, the x-axes in Figs. 1(d)–1(f) and 2(c) are labeled by λ using the conversion $\delta\lambda/\lambda_0 = \delta x/x_0$.)

As mentioned above, the Fourier transform

$$\tilde{I}(t) = \int dx \exp(-it\omega_0 x/x_0) I(x) \quad (2)$$

is found to possess three peaks: the main one, at $t = 0$, and two satellites, Fig. 2(a). We will show that these satellites occur at $|t| = \tau = \delta l/c$. We will also explain the fact that the shapes of the three peaks in Fig. 2(a) are nearly identical. Because of the latter, the amplitude of the oscillations in $I(x)$ is fully characterized by the relative height of the main and the satellite peaks. Therefore, we define the visibility factor by

$$V = 2|\tilde{I}(\tau)|/\tilde{I}(0). \quad (3)$$

Next, we note that the central row of the CCD image in Fig. 1(d)–1(f) is generated by the sources situated on the pinhole's diameter. Thus, instead of two-dimensional vector $\mathbf{r}$, it suffices to use the linear coordinate y along the magnified image of such a diameter, of length $D_s = M_2 D$, at the spectrometer input slit.

The intensity of the CCD image averaged over a large time $T_{\rm im}$ is a result of interaction of the original PL signal $E(t, y)$ with two linear devices, the MZ interferometer and the spectrometer. It is convenient to do the calculation of their combined effect in the frequency domain. We define the Fourier amplitudes $\tilde{E}(\omega_j, y) = \langle E(t, y) \exp(i\omega_j t)\rangle$, for a set of frequencies $\omega_j = 2\pi j/T_{\rm im}$. A straightforward derivation leads to

$$I(x) = \int_{-D_s/2}^{D_s/2}\int_{-D_s/2}^{D_s/2} dy_1 dy_2 \sum_{\omega_j} |1 + \exp(i\omega\tau)|^2 \tilde{E}(\omega_j, y_1) \times \tilde{E}(-\omega_j, y_2) f_s(x, \omega_j, y_1) f_s(x, \omega_j, y_2), \quad (4)$$

where

$$f_s(x, \omega, y) = \frac{\sin(\pi N z)}{\pi z}, \qquad z = \frac{\delta\omega - By}{\omega_0} + \frac{\delta x}{x_0} \quad (5)$$

is the response function of the spectrometer, which is obtained from the standard formula for the diffraction grating of N grooves by expansion in $\delta\omega$ and δx. Parameter B is determined by the linear dispersion of the spectrometer $A = 1.55$ nm/mm, via the relation $B = 2\pi cA/\lambda_0^2$. After algebraic manipulations with Eqs. (1), (2), (4), and (5), we get the following expression for the case of practical interest, $|t| < 2\pi N/\omega_0$:

$$\tilde{I}(t) \propto \int_0^{D_s} \frac{dy}{yt} \sin\left[\frac{1}{2}(D_s - |y|)Bt\right] \sin\left[\left(\frac{2\pi N}{\omega_0} - |t|\right)\frac{B}{2}y\right] \times \left[g(t, y) + \frac{1}{2}g(t - \tau, y) + \frac{1}{2}g(t + \tau, y)\right]. \quad (6)$$

The three-peak structure of $\tilde{I}(t)$ described above stems from the three terms on the last line of Eq. (6). The width of each peak is exactly the coherence time τ_c. The peaks are well separated at $\tau \gg \tau_c$ and their shape is nearly identical if τ_c is sufficiently small. The heights $\tilde{I}(0)$ and $\tilde{I}(\tau)$ of the peaks are determined by the first and the second terms on the last line of Eq. (6), and so

$$V = \frac{(1 - \Delta)\int_0^1 z^{-1}\sin[F(1 - \Delta)z]\sin[F\Delta(1 - z)]\tilde{g}(z)dz}{F\Delta\int_0^1 z^{-1}\sin(Fz)\sin(1 - z)\tilde{g}(z)dz},$$
$$F \equiv \frac{\pi NAD_s}{\lambda_0}, \qquad \tilde{g}(z) \equiv g\left(0, \frac{zD}{M_1}\right), \qquad \Delta \equiv \frac{\delta l}{N\lambda_0}. \quad (7)$$

To understand the implications of this formula, consider first the case of an infinite diffraction grating, $N \to \infty$. Here $\Delta \to 0$, $F \to \infty$ but the product $F\Delta = \pi AD_s\delta l/\lambda_0^2$ remains finite. For the visibility we get

$$V = |\sin(F\Delta)|/F\Delta, \quad (8)$$

so that function $V(\delta l)$ has a periodic sequence of nodes at $\delta l = n\lambda_0^2/(AD_s)$, where $n = 1, 2, \ldots$, and does not depend on ξ. Equation (8) is reminiscent of the Fraunhofer formula for diffraction through a slit of width D_s.

In reality, N is large but finite. In this case, the dependence on ξ does show up. Thus, for $M\xi \ll \lambda_0/AN$, where $M = M_1M_2$, Eq. (7) reduces to

$$V = \frac{1 - \Delta}{f\Delta}|\sin(f\Delta)|, \qquad f = \frac{\pi NA}{\lambda_0}(M_2D - M\xi). \quad (9)$$

To understand the origin of Eqs. (8) and (9), consider the signal at the center of the CCD image, at point x_0. It is created by interference between all pairs of elementary input sources whose coordinates $y_1 = y + \delta y$ and $y_2 = y - \delta y$ differ by no more than $\min\{M\xi, \lambda_0/AN\}$. What contributes to the image is the Fourier harmonic of such sources shifted by $\delta\omega = By$ with respect to the central frequency ω_0, cf. Equation (5). The spread of y across the pinhole results into the spread of $|\delta\omega| \lesssim B(D_s - \delta y)$. If $M\xi \ll \lambda_0/AN$, then $D_s - \delta y = M_2D - M\xi$ plays the role of the effective pinhole diameter in this measurement. The resultant formula for visibility, Eq. (9), is therefore similar to the Fraunhofer formula for diffraction through a slit of this *effective* width.

We compared experimental $V(\delta l)$ with the above theory treating ξ and M_2 as adjustable parameters. Instead of

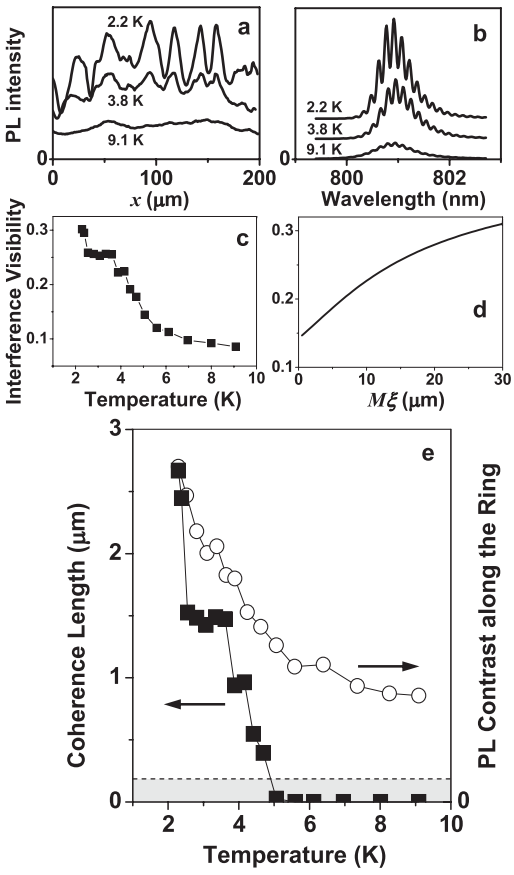

FIG. 3. (a) Variations of the indirect exciton PL intensity along the external ring at $T = 2.2$, 3.8, and 9.1 K. (b) Interference profiles at $T = 2.2$, 3.8, and 9.1 K. (c) Visibility of the interference fringes vs T. (d) Calculated visibility as a function of the coherence length for $M_2 = 1.7$. (e) The exciton coherence length (squares) and contrast of the spatial intensity modulation along the ring (circles) vs T. The shaded area is beyond experimental accuracy. $V_g = 1.24$ V, $P_{\rm ex} = 0.7$ mW for all the data; $D = 50$ μm, and $\delta l = 4.2$ mm for the data in (b)–(e).

using the approximate Eq. (9), we evaluated Eq. (7) numerically. In agreement with Eq. (9), V was found to be most sensitive to ξ for Δ not too close to either zero or unity. It also happened that ξ was of the same order of magnitude as λ_0/ANM, and so the conditions for its estimation were nearly optimal.

As seen in Fig. 2(d) and 2(e), there is a good agreement between the theory and the experiment. The measured $V(T)$, Fig. 3(c) and the calculated $V(\xi)$, Fig. 3(d) allow us to obtain the coherence length $\xi(T)$. Figure 3(e) shows that the coherence length increases sharply at T below a few Kelvin. Intriguingly, the increase of ξ is in concert with the MOES formation.

Naively, the interference pattern of an extended source of length ξ washes out when $\xi\delta k \sim \pi$, where δk is a spread of the momentum distribution. For $\xi \sim 2$ μm [Fig. 3(e)], this gives $\delta k \sim 10^4$ cm^{-1}, which is much smaller than the spread of the exciton momentum distribution in a classical exciton gas $\delta k_{cl} \sim \hbar^{-1}\sqrt{2mk_BT} \approx 3 \times 10^5$ cm^{-1} at $T = 2$ K. In turn, this corresponds to a spread of the exciton energy distribution $\hbar^2\delta k^2/2m \sim 1$ μeV, which is much smaller than that for a classical exciton gas $\delta E_{cl} \sim k_BT \approx 200$ μeV at $T = 2$ K. It may also be interesting to estimate the exciton phase-breaking time $\tau_\phi = \xi^2/D_x$, where $D_x \sim 10$ cm^2/s [19] is the exciton diffusion coefficient. Using again $\xi = 2$ μm, we get τ_ϕ of a few ns. In comparison, the inverse linewidth $\tau_c \sim 1$ ps.

Let us now discuss physical mechanisms that may limit ξ and τ_ϕ. Since $\tau_{\rm rec} \sim 40\,{\rm ns} \gg \tau_\phi$, the effect of exciton recombination on the phase-breaking time is negligible. Next, the excitons are highly mobile, as evidenced by their large diffusion length, ca. 30 μm [20]; therefore, ξ is not limited by disorder localization. The coherence length may also be limited by inelastic collisions of excitons with phonons and with each other. For the high exciton densities $n \sim 10^{10}$ cm^{-2} in our experiments, the dominant ones are the latter [21]. Note also that spontaneous coherence we report arises in a cold thermalized exciton gas (the lifetime $\tau_{\rm rec}$ of the indirect excitons is much longer than their thermalization time to $T = 2$ K, $\sim$1 ns [9]). Since coupling of the indirect excitons to photons is negligible coherence emerging in the cold gases of indirect excitons is similar to coherence in cold matter and is different from the laserlike coherence due to a macroscopic coherent optical field [22].

Theoretical calculation of ξ is yet unavailable. It is expected however that inelastic processes should vanish at $T = 0$. Our findings call for developing a quantitative theory of phase-breaking processes in nonclassical exciton gases at low temperatures when the thermal de Broglie wavelength is comparable to the interparticle separation. In view of the exciting phenomena uncovered in both fermionic [23] and bosonic [24–26] systems at low temperatures, one can expect that rich physics may follow.

This work is supported by NSF Grant DMR-0606543, ARO Grant W911NF-05-1-0527, and the Hellman Fund. We thank K. L. Campman for growing the high quality samples, M. Hanson, A. L. Ivanov, J. Keeling, L. S. Levitov, L. J. Sham, B. D. Simons, and A. V. Sokolov for discussions; G. O. Andreev, A. V. Mintsev, and E. Shipton for help in preparing the experiment.

[1] D. S. Chemla and J. Shah, Nature (London) **411**, 549 (2001).
[2] X. Marie, P. Le Jeune, T. Amand, M. Brousseau, J. Barrau, M. Paillard, and R. Planel, Phys. Rev. Lett. **79**, 3222 (1997).
[3] D. Birkedal and J. Shah, Phys. Rev. Lett. **81**, 2372 (1998).
[4] W. Langbein, J. M. Hvam, and R. Zimmermann, Phys. Rev. Lett. **82**, 1040 (1999).
[5] S. Haacke, S. Schaer, B. Deveaud, and V. Savona, Phys. Rev. B **61**, R5109 (2000).
[6] L. V. Butov, J. Phys. Condens. Matter **16**, R1577 (2004).
[7] L. V. Keldysh and A. N. Kozlov, Zh. Eksp. Teor. Fiz. **54**, 978 (1968) [Sov. Phys. JETP **27**, 521 (1968)].
[8] M. M. Dignam and J. E. Sipe, Phys. Rev. B **43**, 4084 (1991).
[9] L. V. Butov, A. L. Ivanov, A. Imamoglu, P. B. Littlewood, A. A. Shashkin, V. T. Dolgopolov, K. L. Campman, and A. C. Gossard, Phys. Rev. Lett. **86**, 5608 (2001).
[10] L. V. Butov, A. C. Gossard, and D. S. Chemla, Nature (London) **418**, 751 (2002).
[11] L. V. Butov, L. S. Levitov, A. V. Mintsev, B. D. Simons, A. C. Gossard, and D. S. Chemla, Phys. Rev. Lett. **92**, 117404 (2004).
[12] R. Rapaport, G. Chen, D. Snoke, S. H. Simon, L. Pfeiffer, K. West, Y. Liu, and S. Denev, Phys. Rev. Lett. **92**, 117405 (2004).
[13] Th. Östereich, T. Portengen, and L. J. Sham, Solid State Commun. **100**, 325 (1996).
[14] B. Laikhtman, Europhys. Lett. **43**, 53 (1998).
[15] A. Olaya-Castro, F. J. Rodriguez, L. Quiroga, and C. Tejedor, Phys. Rev. Lett. **87**, 246403 (2001).
[16] R. Zimmermann, Solid State Commun. **134**, 43 (2005).
[17] R. Loudon, *The Quantum Theory of Light* (Oxford University Press, New York, 2000), 3rd ed..
[18] M. O. Scully and M. S. Zubairy, *Quantum Optics* (Cambridge University Press, Cambridge, England, 1997).
[19] A. L. Ivanov, L. E. Smallwood, A. T. Hammack, Sen Yang, L. V. Butov, and A. C. Gossard, Europhys. Lett. **73**, 920 (2006).
[20] L. S. Levitov, B. D. Simons, and L. V. Butov, Phys. Rev. Lett. **94**, 176404 (2005).
[21] A. L. Ivanov, P. B. Littlewood, and H. Haug, Phys. Rev. B **59**, 5032 (1999).
[22] For a review, see P. B. Littlewood, P. R. Eastham, J. M. J. Keeling, F. M. Marchetti, B. D. Simons, and M. H. Szymanska, J. Phys. Condens. Matter **16**, S3597 (2004).
[23] B. L. Altshuler, P. A. Lee, and R. A. Webb, *Mesoscopic Phenomena in Solids*, edited by V. M. Agranonich and A. A. Maradudin (North-Holland, Amsterdam, 1991).
[24] M. H. Anderson, J. R. Ensher, M. R. Matthews, C. E. Wieman, and E. A. Cornell, Science **269**, 198 (1995).
[25] C. C. Bradley, C. A. Sackett, J. J. Tollett, and R. G. Hulet, Phys. Rev. Lett. **75**, 1687 (1995).
[26] K. B. Davis, M. O. Mewes, M. R. Andrews, N. J. Vandruten, D. S. Durfee, D. M. Kurn, and W. Ketterle, Phys. Rev. Lett. **75**, 3969 (1995).